E. OVODOK,[1] V. KORMOSH,[2] V. BILANYCH,[3] M. IVANOVSKAYA[1]

[1] Laboratory of Thin Films Chemistry of Research Institute for Physical Chemical Problems, Belarusian State University
(Minsk, Belarus)

[2] Institute of Analytical Technique, Uzhhorod National University
(46, Pidhirna Str., Uzhhorod, Ukraine)

[3] Department of Applied Physics, Faculty of Physics, Uzhhorod National University
(46, Pidhirna Str., Uzhhorod, Ukraine; e-mail: vbilanych@gmail.com)

UDC 539

ACETONE VAPOR SENSORS BASED ON TIN DIOXIDE DOPED BY Au NANOPARTICLES

The effect of nano-sized gold particles on the adsorption-sensitive properties of SnO_2–Au sensors under the detection of acetone vapors has been studied. Different techniques for the preparation of SnO_2–Au nanocomposites with an average Au particle size of 2 nm were applied. It has been found that a fivefold increase in the sensor response to acetone vapors and threshold sensitivity (C_{lim}) of 0.1 ppm are achieved by adding gold to tin dioxide in the colloidal form during synthesis. While adding gold in ion form (Au (III)) leads to a growth of the sensor response to acetone vapors by 2.7 times and defines C_{lim} of 0.2 ppm. The slope of the calibration curves of the SnO_2–Au sensors allows registering acetone vapors at concentrations ranging from C_{lim} to 5 ppm. This concentration range can be used for the express diagnostics in diabetes. The enhanced sensitivity of SnO_2–Au sensors to acetone vapors can be explained by an increase in the adsorption-catalytic activity of tin ions as a result of the modifying effect of sulfate groups and the envolving of highly dispersed gold in the adsorption – catalytic process of oxidation of acetone molecules.

K e y w o r d s: SnO_2, gold nanoparticles, acetone gas sensors.

1. Introduction

To diagnose various diseases and to monitor the health status of patients with certain chronic illnesses, different methods to identify markers (substances accompanying these diseases in the human body) are used [1, 2]. In particular, the possibilities of determining some markers in human exhale in dental diseases and diabetes are being widely studied [3, 4]. Many of these biomarker substances are present in the exhale of a healthy person, but their concentration increases in the case of a disease.

When diagnosing diabetes, acetone vapors are determined in the exhale of a person, since the concentration of other substances is considerably lower. Different methods of determination of acetone vapors are being developed. In recent years, along with the most common method of chromatography [gas chromatography with a plasma photometric detector (PPD)],

intensive work is underway to establish the possibility to determine acetone vapors using sensors [5]. Metal oxide resistive sensors are predominantly studied among different types of sensors [5]. An intensive experimental work has been carried out to test different metal oxide materials as acetone sensors [5, 6]. The interest in these type of sensors is caused by the fact that this might be a new area of their application. The research being carried out should show how this direction will be applicable in the practice of express diagnostics.

The search for promising materials for acetone vapor sensors appeared mainly empirically. Different types of oxide materials doped with activating additives have been tested [5–7]. It was shown that the most promising are WO_3- and ZnO-based materials. However, other semiconducting metal oxides may also be applicable. SnO_2 is a traditional and widely used material in the production of gas sensors for toxic and flammable gases. It is suitable for the machine technology of sensor manufacturing. Tin diox-

ide is characterized by high thermal and chemical stabilities and has a wide band gap of 3.6 eV. The gas sensitivity of SnO_2-based sensors is significantly improved, when doped with different additives [8, 9].

Nano-sized oxide materials are used for acetone sensors. Different methods for the synthesis of nano-sized metal oxides have been developed. This allows one to obtain particles with different morphology: rods, bars, sticks, threads, fibers, tubes, thin sheets and strips, flowers, petals, porous structures, *etc.* All these anisotropic particles with the size ranging from 120–500 nm to 1–2 μm consist of small isotropic particles, the diameter of which corresponds to the nanometer range (less than 100 nm). Various organic additives are used in the synthesis of anisotropic nanoparticles of metal oxides (citrate ions, dimethylformamide, pluronic, PVP, surfactants). Such syntheses are carried out in an ethanol/H_2O mixture by the template or carbon-thermal method. The presence of C-containing substances not only promotes the growth of particles of a given shape, but also contributes to the formation of an oxide structure with a high concentration of structural defects. Partial reduction of oxides leads to the formation of oxygen vacancies and ions with a lower than the main oxidation state. In addition, the synthesis with carbon-containing additives promotes the formation of metastable phases of metal oxides (WO_3, In_2O_3, ZnO), which may have the adsorption and conductive properties different from that of the stable phases [5–7]. However, the influence of these factors remains poorly studied. It is known that the highest sensitivity threshold (0.007–0.067 ppm) to acetone vapors is achieved by doping SnO_2 with carbon and nitrogen [8, 9].

In the synthesis of SnO_2 materials for acetone sensors, $SnCl_4$ and $SnCl_2$ are most often used as precursors. Although it is known that the use of other tin salts makes it possible to exclude the negative effect of chloride ion impurities on the adsorption-catalytic properties of SnO_2-sensors. The modifying effect of sulfate ions on the surface state of different metal oxides is known. Sulfate ions improve their catalytic properties in oxidation reactions [10–13].

This work is aimed at the study of the effect of the nano-sized gold particles on the gas sensitivity of the SnO_2–Au nanocomposites to acetone vapors. A distinctive feature of the studied SnO_2–Au nanocomposites is that both components (SnO_2, Au) are nano-

sized. Tin dioxide was synthesized via $SnSO_4$ as a starting material according to the previously developed technique that allows one to obtain nano-sized tin dioxide particles with surface modified by sulfate groups [11].

2. Materials and Experiments

2.1. Methods of synthesis

Tin dioxide (SnO_2) was synthesized by the sol-gel method via $SnSO_4$ salt. The synthesis technique includes a preliminary treatment of $SnSO_4$ (20 g) with 20 ml of H_2SO_4 (98 wt.%) under the heating at 200 °C for 10 min. At the end of the reaction, the solution was diluted with distilled water up to 200 ml. Then the ammonia solution (5 vol.%) was added dropwise until pH 8 was reached. The obtained precipitate was separated by a the centrifugation and washed 3 times with distilled water. Next, 50 ml of distilled water and 0.1 ml of sulfuric acid (98 wt.%) were added to the precipitate. The suspension was ultrasonicated ($f = 22$ kHz, $P = 130$ W) for 2 minutes and $SnO_2 \cdot nH_2O$ sol was prepared. According to the TEM analysis, after the heating, $SnO_2 \cdot nH_2O$ xerogel at 600 °C, SnO_2 powder was obtained with a narrow particle size distribution and the average diameter $d \approx 5.5$ nm [10–12].

The SnO_2–Au nanocomposites were obtained by adding the colloid solution of gold or $HAuCl_4$ solution into $SnO_2 \cdot nH_2O$ sol in the quantity corresponding to 0.15 at.% of Au relative to SnO_2. The formation of SnO_2–Au nanocomposite occurs under the thermal treatment of hydroxylated amorphous tin oxide containing nano-sized Au particles or Au ions, respectively.

To obtain the colloidal solution of gold, $AuCl_4^-$ ions were reduced by sodium borohydride in the presence of 5-(2-mercaptoethyl) tetrazole stabilizer [14]. The size of Au particles in a colloidal solution was $1.9 \pm \pm 0.1$ nm. Au particles retain their size, when added to SnO_2–Au nanocomposite. The sample obtained with the use of the gold colloidal solution is denoted as SnO_2–Au^0.

No gold particles were detected by the TEM method in SnO_2–Au nanocomposites obtained by adding Au (III) into the $SnO_2 \cdot nH_2O$ sol. This can be explained by both the small size and the specific morphology of the gold particles. According to the XPS data presented below, the gold content on the sur-
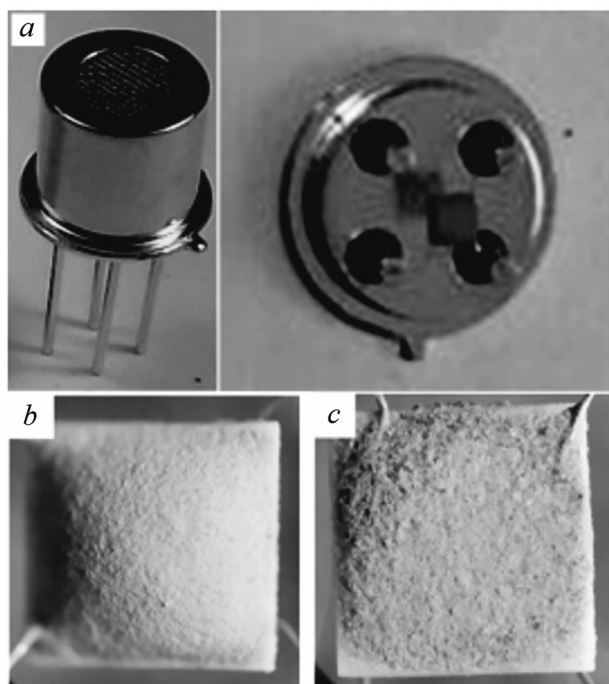
Fig. 1. Photographs of the sensor (a) and sensing element of SnO_2 (b) and SnO_2–Au^{III} (c)

face of this sample is 5 times lower than the amount added into the sol during the synthesis and constitutes 0.03 at.%. This result may indicate the encapsulation of Au particles with tin dioxide under conditions of joint formation of the SnO_2–Au nanocomposite from a colloidal solution of $SnO_2 \cdot nH_2O$ + Au^{III} during thermal dehydration. The optical spectrum of such composite allows us to suggest that the gold particles are about 2 nm in size. This sample is denoted as SnO_2–Au^{III} (see Tabl. 1).

2.2. Methods of characterization

The samples were characterized by the transmission electron microscopy (TEM), infrared (IR) spec-

Table 1. **The samples studied in this paper**

Sensing material	Au stat	Stabilizer of Au nanoparticles	d_{Au}, nm
SnO_2	–	–	–
SnO_2–Au^0	Nanoparticles	5-(2-mercapto-ethyl)-tetrazole	1.9 ± 0.1
SnO_2–Au^{III}	$HAuCl_4$	–	~ 2

troscopy, X-ray photoelectron spectroscopy (XPS), and UV-Vis spectroscopy. The grain size distribution was ascertained on a LEO-906E transmission electron microscope. The IR-spectra were recorded on an AVATAR-330 (Thermo Nicolet) spectrometer equipped with a Smart Diffuse Reflectance accessory in the wavelength range of 400–4000 cm^{-1}. The XPS spectra were measured from the surface of the original samples. XPS signals were recorded by using a Thermo Scientific K-Alpha XPS system (Thermo Fisher Scientific Inc., UK) equipped with a microfocused monochromatic Al Kα X-ray source (1486.68 eV). UV-Vis absorption spectra were recorded by using a Shimadzu UV-2550 spectrophotometer.

2.3. Manufacturing the sensors and measuring their characteristics

To manufacture the sensing elements, the SnO_2 and SnO_2–Au powders were ground thoroughly in ethanol to obtain the corresponding pastes. The pastes were used to form thick-film layers on microplatforms for sensors. The general view of the sensor and sensing element is depicted in Fig. 1. The thickness of the sensitive layer was about 150 μm.

The standard microplatforms made of aluminium oxide substrates with platinum heater and measuring electrodes were used. The microplatform width was 1.6 mm, and the thickness was 0.25 mm. The sensing elements were mounted in a standard casing (see Fig. 1, a). The resistance of the sensors in wet air (R_0) and standard acetone-air mixtures (R_g) were measured in a constant voltage mode. The temperature-dependent responses of the sensors were mainly acquired at 50 ppm of acetone vapors.

3. Results and Discussionl

3.1. Gas-sensing properties

The dependence of the sensor response on the working temperature, when detecting 50 ppm acetone vapors, are presented in Fig. 2. Adding gold into the nanocomposites leads to a significant growth of the output signal of the SnO_2-based sensors. The response increases by 5 times in the case of SnO_2–Au^0 sensors and by 2.7 times in the case of SnO_2–Au^{III} sensors in comparison with SnO_2 sensors. The optimal temperature interval for the detection of acetone vapors is at higher temperature for sensors contain-
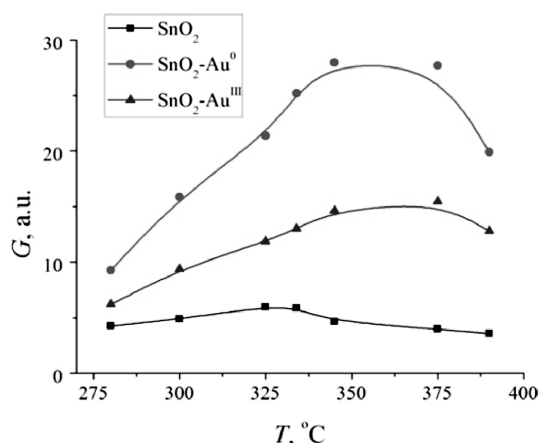
Fig. 2. The sensor response vs working temperature graphs of the SnO_2, SnO_2–Au^{III}, and SnO_2–Au^0 sensors under detection of acetone vapors (50 ppm)

ing gold particles. Effective acetone detection is observed for these sensors in the interval from 300 to 390 °C with a maximum at 340–370 °C. The wide temperature interval of the acetone vapors detection might indicate the implementation of an additional and more efficient detection mechanism on the surface of the SnO_2–Au sensors in comparison with the SnO_2 sensor.

Dynamic parameters can indicate different mechanisms of acetone detection by SnO_2–Au^0 sensor. Figure 3 shows the dependences of the sensor responses to 10 ppm of acetone vapors vs time. The response time measured for SnO_2–Au sensors is short enough (3–6 s). Recovery to 70% of initial parameters of SnO_2–Au^0 sensors, after the end of the gas supply, occurs quickly, and then it slows down and becomes as slow as for SnO_2 sensors. This may indicate the difficulty in the desorption of acetone molecules or products of its oxidation. The changes in the electrical characteristics of SnO_2–Au^0 sensors can be described by two of the known mechanisms: the direct adsorption-desorption of volatile organic compounds on the SnO_2 surface [7, 15] and oxidation-reduction, the so-called "oxygen vacancy model" [16]. It was found that acetone molecules are adsorbed at the SnO_2 surface on tin ions by the oxygen of the carbonyl group with the transfer of electron density to the oxide [15, 17]. The intermediate and final products of the adsorption of ketones on oxides have been studied in [18]. Surface acetate is the most common product of the
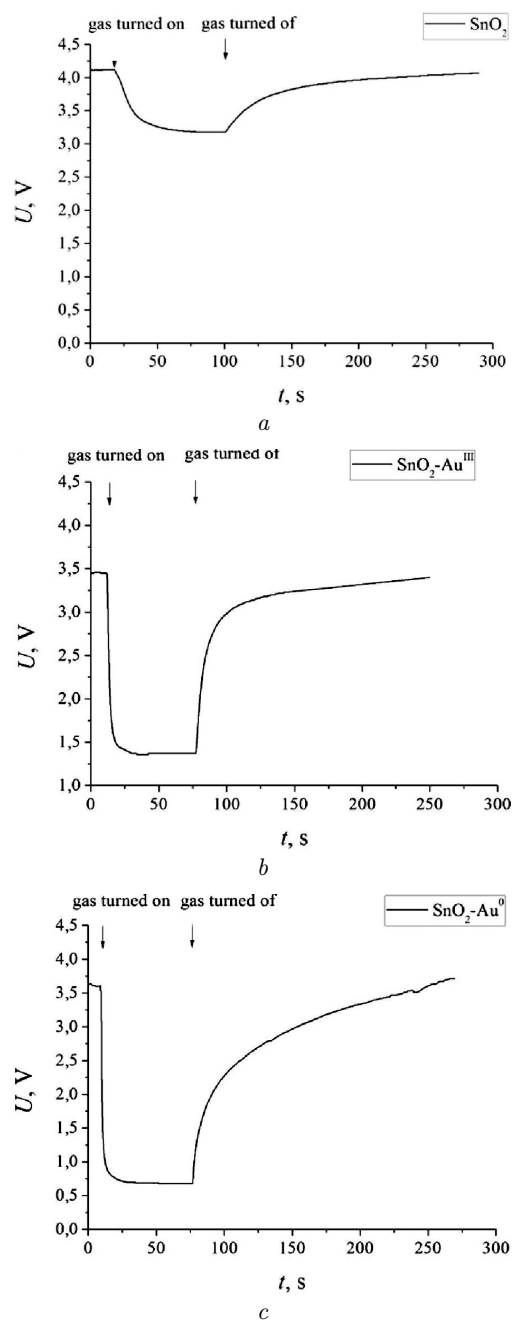

Fig. 3. Dynamic characteristics of the SnO_2 (*a*), SnO_2–Au^{III} (*b*), and SnO_2–Au^0 (*c*) sensors under detection of acetone vapors (10 ppm)

chemisorption of ketones on the surfaces of oxides at 350 °C [17, 19].

The study of sensors for the determination of low concentrations of acetone vapors (less than 5 ppm)

Table 2. **The samples studied in this paper**

Sample	Au, at%, (XPS)	BE, eV Au $4f_{5/2}$	α = BE Sn $3d_{5/2}$ KE Sn MNN (XPS)	BE, eV S 2p	S–O (IR)
SnO$_2$–Au^0 0.15 at%	0.12	84.0 (Au^0)	SnO$_2$, Sn^{2+}, impurity [SnO$_5$V$_0$]	169.3 SO$_4^{2-}$	SO$_4^{2-}$, bident SO$_3^{2-}$, monodent
SnO$_2$–Au^{III} 0.15 at%	0.03	83.9 (Au^0) 84.9 (Au$^+$Au$_n$)	SnO$_2$	169.3 SO$_4^{2-}$	SO$_4^{2-}$, bident
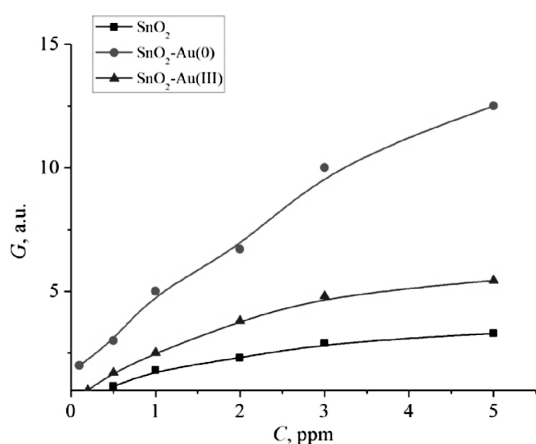
Fig. 4. Dependences of the response of SnO$_2$, SnO$_2$–Au^0, and SnO$_2$–Au^{III} sensors on the concentration of acetone vapors

deserves a special attention. This interval can be used for the express diagnosis of diabetes. As is known, the acetone content is 0.3–0.9 ppm in the exhale of a healthy person. The acetone concentration in the exhale may grow up to 1.8–5.0 ppm for a person with diabetes. Figure 4 shows the dependences of the response of sensors on the concentration of acetone vapors. The slopes of the the curves for SnO$_2$–Au sensors allow one to distinguish between small changes in the acetone vapor concentration from a minimal detectable value up to 5 ppm. The SnO$_2$ sensors do not possess such ability.

3.2. Structural features

A significant difference in the properties of the SnO$_2$–Au^0 and SnO$_2$–Au^{III} sensors is observed. The structural features of these nanocomposites are considered to explain the differences in the properties of the sensors. The structural characteristics of these nanocomposites were studied in details in our previous work [12]. The states of Au and the surface of SnO$_2$ in

SnO$_2$–Au^0 and SnO$_2$–Au^{III} nanocomposites are presented in Table 2. Some results on the study of samples by the XPS, Auger, and IR spectroscopy methods are also presented.

According to the XPS data, the gold content on the surface of the SnO$_2$–Au samples is different. The amount of 0.12 at.% was found in SnO$_2$–Au^0 sample and 0.03 at.% – in SnO$_2$–Au^{III} sample. The Au $4f$ and Au $3d$ lines in the spectra of SnO$_2$–Au^0 and SnO$_2$–Au^{III} samples have low intensity and large width (FWHM $3d_{5/2} \sim 4$ eV), which is a result of the small size of gold particles. The shape of the Au $4f_{7/2}$ and Au $4d_{5/2}$ lines with the maxima at 84.0 ± 0.1 and 335.2 ± 0.1 eV indicates the occurrence of the Au^0 state in the SnO$_2$–Au^0 sample. In the XPS spectrum of SnO$_2$–Au^{III} sample, the Au $4d_{5/2}$ line is hardly distinguishable, whereas two Au $4f_{7/2}$ low-intensity peaks with BE = 83.9 and 84.9 eV are registered. The first peak corresponds to the Au^0 state. The second one can be attributed to Au$^+$ state [20]. Thermal treatment at 600 °C should have evoked the complete transformation of Au^{III} ions to the metal state of gold (Au^0). However, this conversion might be hindered in SnO$_2 \cdot n$H$_2$O + Au^{III} amorphous system, by resulting in the stabilization of the partially oxidized state of gold on the surface of gold clusters – (Au$_n$)Au$^+$.

A slight shift in the position of the maximum of the Sn $3d_{5/2}$ line at 487.3 ± 0.1 eV toward lower binding energies in the spectrum of SnO$_2$–Au$_0$ sample may be caused by imperfections of its structure caused by the appearance of oxygen vacancies [SnO$_5$V$_0$] in the environment of tin cations [21]. A large oxygen deficiency may cause the appearance of Sn^{2+} cations in the SnO$_2$ structure [22].

The modified Sn Auger parameter (α = BE Sn $3d_{5/2}$ + KE Sn MNN AES) [20] is a more reliable indicator of tin state. The measured value of this parameter indicates the occurrence of SnO$_2$ phase in

Table 3. **Comparison of the properties of some acetone sensors**

Material	Morphology	C_{Lim}, ppm	Temp. $^\circ$C	$G = R_0/R_g$, 50 ppm	Type of sensor	Ref.
SnO_2	*NP, $d_{SnO_2} = 4$–6 nm	0.5	320	6	Planar electrode substrate	This paper
SnO_2–Au	NP, $d_{SnO_2} = 4$–6 nm $d_{Au} = 1.9$ nm	0.1	340	30	Planar electrode substrate	Same
SnO_2–Au^{III}	NP, $d_{SnO_2} = 4$–6 nm $d_{Au} = 2$ nm	0.2	340	16	Planar electrode substrate	”
SnO_2	Multichannel **NFs $d = 150$–250 nm		310	11.4	Alumina substrate	[27]
SnO_2	Hollow micro-spheres 600–900 nm	–	280	–	Ceramic tube	[28]
Au–SnO_2	$d_{SnO_2} = 20$–50 nm	5	220	30		
SnO_2	NFs $d = 150$ nm	–	200	6	Planar electrode substrate	[29]
Rh–SnO_2	$d_{SnO_2} = 6$–10 nm	1	200	60		
SnO_2	NFs $d = 120$–150 nm	5	200	4	Planar electrode substrate	[30]
Ru–SnO_2	$d_{SnO_2} = 6$–9 nm	0.5	200	40		
SnO_2	Nanospheres,		290	12	Ceramic tube	[30]
Au/SnO_2	$d_{SnO_2} = 7$–12 nm,	5	280	71		
Pd/SnO_2	$d_{Au} = 3$–10 nm	–	250	42		
PdAu/SnO_2		0.1	250	109		

*NP – nanoparticles; **NFs – nanofibers.

SnO_2 and SnO_2–Au^{III} samples. In addition, this does not exclude Sn^{2+} admixture occurred in SnO_2–Au^0 sample.

The S $2p$ peak with BE ≈ 169.3 eV attributed to SO_4^{2-} ion is registered in the XPS spectra of the samples [23]. The sulphur content was estimated on the surface of the samples to be 2.7–3.1 at.%.

IR spectroscopic data confirm the presence of SO_x-groups in the samples. Bidentate bound sulfate groups SO_4^{2-} predominate [24]. The line at 820 cm^{-1} in the spectrum of SnO_2–Au^0 sample can be an attribute of the monodentate O-coordinated SO_3 group on SnO_2 surface. Annealing the samples at 600 °C also promotes the formation of sulfate groups on the surface of tin dioxide.

The presence of sulfate-sulfite groups in the samples can be explained by the adsorption of SO_2 on SnO_2 surface. Sulphate ions, included in $SnO_2 \cdot nH_2O$ sol from precursors ($SnSO_4$, H_2SO_4), are source of SO_2. In the case of SnO_2–Au^0 sample, the S-containing stabilizer of Au colloidal particles 5-(2-mercaptoethyl)tetrazole is an additional source of

SO_2. Thermal destruction of this substance occurs in stages [25]. A large amount of gaseous products is formed as a result of the destruction of the tetrazole ring. Sulfur removal occurs at the last stage (500–600 °C). These factors have a significant effect on the formation of the crystal structure and surface of Au and SnO_2 particles from amorphous $SnO_2 \cdot nH_2O$ xerogel. These factors also explain the appearance of structural defects, primarily oxygen vacancies and Sn^{2+} cations in the SnO_2–Au^0 sample, since structural oxygen from $SnO_2 \cdot nH_2O$ and SnO_2 can take part in the oxidation of the stabilizer of Au colloidal particles. Disordered fragments of the tin dioxide structure (Sn_nO_{2n-1}) and the Au/Sn_nO_{2n-1} boundaries can act as oxygen activation centers.

It is known [13, 26] that the adsorbed forms of SO_2 change the nature of active centers on the surface of metal oxides. They increase the strength of Lewis acid sites (surface metal ions) due to the induction effect. The induction effect consists in a shift of the electron density from tin cations by SO_2 molecules.

Thus, two factors – the defectiveness of the SnO_{2-x} structure and the presence of adsorbed forms of SO_2 allows explaining the high sensitivity of SnO_2–Au^0 sensors to acetone vapors. The higher response of the SnO_2–Au^0 sensors as compared to the SnO_2–Au^{III} sensors is explained by the high defectiveness of the SnO_2 surface and the high concentration of Au on their surface.

Table 3 shows some parameters of the sensors studied in this work in comparison with other SnO_2 sensors. In the selected tin dioxide sensors, the synthesis of the sensitive material was carried out, by using carbon-containing organic substances and polymers. The sensors based on SnO_2 without dopants and doped with Au are discussed in [27, 28]. For comparison, SnO_2 sensors doped with Ru or Rh [29, 30] are considered. Ruthenium, like gold, is a catalyst for the partial oxidation of organic substances. The catalytic activity of rhodium is poorly studied. The $PdAu/SnO_2$ sensor with a bimetallic additive is characterized by the highest sensitivity threshold to acetone vapors among the SnO_2 sensors doped with noble metals [31].

The SnO_2–Au nanocomposites investigated in this work differ from the materials listed in Table 3 by the smallest sizes of SnO_2 and Au particles, as well as by a low concentration of gold. However, they are highly sensitive to low concentrations of acetone vapors. The threshold sensitivity of SnO_2–Au_0 sensors is comparable to that of $PdAu/SnO_2$ sensor. This bimetallic sensor is characterized by a synergistic effect that increases their sensitivity. Other sensors (Au–SnO_2; Au/SnO_2; Rh–SnO_2; Ru–SnO_2) have a lower threshold sensitivity to acetone.

The response of SnO_2–Au^0 sensor is comparable or less than that of other Au–SnO_2 sensors when detecting 50 ppm acetone. This can be explained by the lower content of Au (0.15 at% or 0.2 wt%.) in SnO_2–Au^0 than in other sensors with higher response – Au/SnO_2, $PdAu/SnO_2$ (0.9507%) [30], Rh–SnO_2 (0.5 mol. % Rh) [30], Ru–SnO_2 (2 mol.% Ru) [31].

4. Conclusions

The addition of colloidal gold with a particle size of 1.9 ± 0.1 nm, stabilized by 5-(2-mercaptoethyl) tetrazole, into the $SnO_2 \cdot nH_2O$ sol enhances the sensitivity of the SnO_2–Au^0 sensors to low concentrations of ace-

tone vapors. The threshold sensitivity of SnO_2–Au^0 sensors to acetone is 0.1 ppm.

The slopes of the concentration curves of SnO_2–Au^0 sensors allow one to detect acetone concentrations in the interval from 0.1 ppm to 5 ppm, which is necessary for the express diagnosis of diabetes.

The high sensitivity of SnO_2–Au sensors to acetone vapors is due to the effect of SO_4^- groups on the adsorption activity of SnO_2 surface and the evolving of highly dispersed Au in the process of oxidation of acetone molecules.

1. D. Hill, R. Binions. Breath analysis for medical Diagnosis. *Inter. J. on Smart Sensing and Intelligent Systems* **5**, 401 (2012).

2. B. Buszewski, M. Kesy, T. Ligor, A. Amann. Human exhaled air analytics: Biomarkers of diseases. *Biomed. Chromatogr.* **21**, 553 (2007).

3. V. Saasa, T. Malwela, M. Beukes, M. Mokgotho, Ch-Pu Liu, B. Mwakikunga. Sensing technologies for detection of acetone in human breath for diabetes diagnosis and monitoring. *Diagnostics* **8**, 12 (2018.

4. M. Righettoni, A. Tricoli. Toward portable breath acetone analysis for diabetes detection. *J. Breath. Res.* **5**, 037109 (2011).

5. M. Masikini, M. Chowdhury, O. Nemraoui. Review-metal oxides: Application in exhaled breath acetone chemiresistive sensors. *J. Electrochem. Soc.* **167**, 037537 (2020).

6. N. Alizadeh, H. Jamalabadi, F. Tavoli. Breath acetone sensors as non-invasive health monitoring systems: A review. *IEEE Sensors Journal* **20**, 5 (2020).

7. S. Americo, E. Pargoletti, R. Soave, F. Cargnoni, M.I. Trioni, G.L. Chiarello, G. Cerrato, G. Cappelletti. Unveiling the acetone sensing mechanism by WO_3 chemiresistors through a joint theory-experiment approach. *Electrochimica Acta* **371**, 137611 (2020).

8. J. Hu, C. Zou, Y. Su, M. Li, Z. Yang, M. Ge, Y. Zhang. One-step synthesis of 2D C_3N_4-tin oxide gas sensors for enhanced acetone vapor detection. *Sens. Actuators B Chem.* **253** 641 (2017).

9. X. Guan, Y. Wang, P. Luo, Y. Yu, D. Chen, X. Li. Incorporating *N* atoms into SnO_2 nanostructure as an approach to enhance gas sensing property for acetone. *Nanomaterials* **9**, 445 (2019).

10. E. Ovodok, M. Ivanovskaya, D. Kotsikau, V. Kormosh, I. Alyakshev. Kotsikau, V. Kormosh, I. Alyakshev. The structure and the gas sensing properties of nanocrystalline tin dioxide synthesized from tin(II) sulphate physics. *Chem. Appl. Nanostr.* 313 (2015).

11. E. Ovodok, M. Ivanovskaya, D. Kotsikau, V. Kormosh, P. Pylyp, V. Bilanych. Structural characterization and gas sensing properties of nano-sized tin dioxide material synthesized from tin(II) sulfate. *Ukr. J. Phys.* **66**, 803 (2021).

12. M. Ivanovskaya, E. Ovodok, T. Gaevskaya, D. Kotsikau, V. Kormosh, V. Bilanych, M. Micusik. Effect of Au nanoparticles on the gas sensitivity of nanosized SnO_2. *Mater. Chem. Phys.* **258**, 123858 (2021).

13. L.M. Kustov, V.B. Kazansky, F. Figueras, D. Tichit. Investigation of the acidic properties of ZrO_2 modified by SO_2^{-4} anions. *J. Catal.* **150**, 143 (1994).

14. C. Guhrenz, A. Wolf, M. Adam, L. Sonntag, S.V. Voitekhovich, S. Kaskel, N. Gaponik, A. Eychmüller. Tetrazole-stabilized gold nanoparticles for catalytic applications. *Z. Phys. Chem.* **231**, 51 (2017.

15. A.A. Abokifa, K. Haddad, J. Fortner, C.S. Lo, P. Biswas. Sensing mechanism of ethanol and acetone at room temperature by SnO_2 nano-columns synthesized by aerosol routes: theoretical calculations compared to experimental results. *J. Mater. Chem. A* **6**, 2053 (2018).

16. A. Tricoli, M. Righettoni, A. Teleki. Semiconductor gas sensors: Dry synthesis and application. *Angew. Chem. Int. Ed.* **49**, 7632 (2010).

17. W. Thoren, D. Kohl, G. Heiland. Kinetic studies of the decomposition of CH_3COOH and CH_3COOD on SnO_2 single crystals. *Surface Sci.* **162**, 402 (1985).

18. P.G. Harrison, B.M. Maunder. Tin oxide surfaces. Part 11. Infrared study of the chemisorption of ketones on tin(IV) oxide. *J. Chem. Soc., Faraday Trans. I* **80**, 1329 (1984).

19. A.-K. Elger, C. Hess. Elucidating the mechanism of working SnO_2 gas sensors using combined operando UV/Vis, Raman, and IR spectroscopy. *Angew. Chem. Int. Ed.* **58**, 15057 (2019).

20. *Practical surface analysis by Auger and X-ray photoelectron spectroscopy.* Edited by D. Briggs, M.P. Seah (John Wiley and Sons Ltd., 1983).

21. Y. Yang, Y. Wang, S. Yin. Oxygen vacancies confined in SnO_2 nanoparticles for desirable electronic structure and enhanced visible light photocatalytic activity. *Appl. Surf. Sci.* **420**, 399 (2017).

22. S. Shi, D. Gao, Q. Xu, Z. Yang, D. Xue. Singly-charged oxygen vacancy-induced ferromagnetism in mechanically milled SnO_2 powders. *RSC Advances* **4**, 45467 (2014).

23. C.L. Lau, G.K. Wertheim. Oxidation of tin: An ESCA study. *J. Vac. Sci. Technol.* **15**, 622 (1978).

24. K. Nakamoto. *Infrared and Raman spectra of inorganic and coordination compounds* (John Wiley & Sons, Ltd., 1986).

25. S.V. Voitekhovich, A. Wolf, C. Guhrenz, A.S. Lyakhov, L.S. Ivashkevich, M. Adam, N. Gaponik, S. Kaskel, A. Eychmueller. 5-(2-Mercaptoethyl)-1H-tetrazole: Facile synthesis and application for the preparation of water soluble nanocrystals and their gels. *Chem. Eur J.* **22**, 14746 (2016).

26. F. Berger, E. Beche, R. Berjoan, D. Klein, A. Chambaudet. An XPS and FTIR study of SO_2 adsorption on SnO_2 surfaces. *Appl. Surf. Sci.* **93**, 9 (1996).

27. T. Wang, S. Ma, L. Cheng, X. Jiang, M. Zhang, W. Li, W. Jin. Facile fabrication of multishelled SnO_2 hollow microspheres for gas sensing application. *Materials Letters* **164**, 56 (2016).

28. Y. Li, L. Qiao, D. Yan, L. Wang, Y. Zeng, H. Yang. Preparation of Au-sensitized 3D hollow SnO_2 microspheres with an enhanced sensing performance. *J. Alloys and Compounds* **586**, 399 (2014).

29. X. Kou, N. Xie, F. Chen, T. Wang, L. Guo, C. Wang, Q. Wang, J. Ma, Y. Sun, H. Zhang, G. Lu. Superior acetone gas sensor based on electrospun SnO_2 nanofibers by Rh doping. *Sensors and Actuators B: Chemical* **256**, 861 (2018).

30. X. Kou, F. Meng, K. Chen, T. Wang, P. Sun, F. Liu, X. Yan, Y. Sun, F. Liu, K. Shimanoe, G. Lu. High-performance acetone gas sensor based on Ru-doped SnO_2 nanofibers. *Sensors and Actuators B: Chemical* **320**, 128292 (2020).

31. G. Li, Z. Cheng, Q. Xiang, L. Yan, X. Wang, J. Xu. Bimetal PdAu decorated SnO_2 nanosheets based gas sensor with temperature-dependent dual selectivity for detecting formaldehyde and acetone. *Sensors and Actuators B: Chemical* **283**, 590 (2019).

Є. Оводок, В. Кормош,
В. Біланич, М. Івановська

НАПІВПРОВІДНИКОВІ ОКСИДИ
МЕТАЛІВ, ЛЕГОВАНІ НАНОЧАСТИНКАМИ
ЗОЛОТА, ДЛЯ ВИКОРИСТАННЯ
В ГАЗОВИХ СЕНСОРАХ АЦЕТОНУ

Досліджено вплив нанорозмірних частинок золота на адсорбційно-чутливі властивості сенсорів на основі SnO_2–Au при детектуванні парів ацетону. Були використані різні методи приготування нанокомпозитів SnO_2–Au із середнім розміром частинок Au 2 нм. Встановлено, що п'ятикратне збільшення відгуку сенсора на пари ацетону та порогова чутливість (C_{lim}) 0,1 ppm досягаються при додаванні золота до діоксиду олова в колоїдній формі в процесі синтезу. Додавання золота в іонній формі (Au(III)) приводить до збільшення відгуку сенсора на пари ацетону в 2,7 рази і визначає C_{lim} 0,2 ppm. Нахил градуювальних кривих сенсорів SnO_2–Au дозволяє реєструвати пари ацетону в діапазоні концентрацій від C_{lim} до 5 ppm. Цей діапазон концентрацій можна використовувати для експрес-діагностики цукрового діабету. Підвищену чутливість SnO_2–Au-сенсорів до парів ацетону можна пояснити підвищенням адсорбційно-каталітичної активності іонів олова в результаті модифікуючої дії сульфатних груп та залучення високодисперсного золота до адсорбційно-каталітичного процесу окислення молекул ацетону.

К л ю ч о в і   с л о в а: SnO_2, наночастинки золота, сенсори ацетону.